

Three-nucleon photodisintegration of ${}^3\text{He}$

R. Skibiński,¹ J. Golak,^{1,2} H. Witała,¹ W. Glöckle,² H. Kamada,³ and A. Nogga⁴

¹*M. Smoluchowski Institute of Physics, Jagiellonian University, PL-30059 Kraków, Poland*

²*Institut für Theoretische Physik II, Ruhr-Universität Bochum, D-44780 Bochum, Germany*

³*Department of Physics, Faculty of Engineering, Kyushu Institute of Technology, 1-1 Sensuicho, Tobata, Kitakyushu 804-8550, Japan*

⁴*Department of Physics, University of Arizona, Tucson, Arizona 85721*

(Received 16 January 2003; published 13 May 2003)

The three-nucleon ($3N$) photodisintegration of ${}^3\text{He}$ has been calculated in the whole phase space using consistent Faddeev equations for the three-nucleon bound and scattering states. Modern nucleon-nucleon and $3N$ forces have been applied, in addition to different approaches to nuclear currents. Phase space regions are localized where $3N$ force effects are especially large. In addition, semi-exclusive cross sections for ${}^3\text{He}(\gamma, N)$, which carry interesting peak structures, have been predicted. Finally, some data for the exclusive $3N$ breakup process of ${}^3\text{He}$ and its total breakup cross section have been compared to theory.

DOI: 10.1103/PhysRevC.67.054002

PACS number(s): 21.45.+v, 24.70.+s, 25.10.+s, 25.40.Lw

I. INTRODUCTION

The reactions ${}^3\text{He}(\gamma, np)p$ and ${}^3\text{He}(\gamma, pp)n$ have been studied experimentally in the past, below and above the pion threshold. In this paper we only consider the energy regime below the pion threshold. In Refs. [1,2] these processes have been investigated in relation to a search for three-body absorption mechanisms or to observe quasideuteron breakup. We refer the reader, for earlier studies, to these two references. Quite a few pioneering theoretical studies have been performed by Laget [3] and applied to these reactions. These calculations are done using a certain class of diagrams consisting of absorption mechanisms of the photon at one, two, and three nucleons and allowing for low order rescattering among the nucleons. Pioneering calculations in the framework of Faddeev equations and based on S -wave spin dependent separable potentials have been carried out in Ref. [4]. There cross sections for the semiexclusive processes ${}^3\text{He}(\gamma, N)$ have been determined.

In a previous paper [5] we investigated the two-body breakup process of ${}^3\text{He}$ (${}^3\text{H}$) with the aim to search for three-nucleon ($3N$) force effects. We found that most of the existing data supported qualitatively the predicted three-nucleon force (3NF) effects, but new precise data would be helpful to challenge theory more strongly.

Here we are mostly interested in kinematically complete $3N$ breakup processes and shall employ rigorous solutions of the Faddeev equations consistently for the $3N$ bound state and the $3N$ continuum. Modern nucleon-nucleon (NN) and 3NF's will be used and mesonic exchange currents (MEC) will be employed either explicitly or in the form of the Siegert approximation. Both forms were previously used and described in Ref. [6] to investigate the p - d capture process. The present investigation focuses on predicting those regions of the $3N$ phase space, where 3NF effects are especially pronounced. Of course, this is based on the present-day 3NF model. We should also remark that we have not yet included explicit $3N$ electromagnetic current operators, which are required by the continuity equation and which may play a role. In case of the Siegert approximation, however, some of them are automatically included.

In addition to the fully exclusive breakup cross section, we also present theoretical predictions for the semiexclusive processes ${}^3\text{He}(\gamma, p)$ and ${}^3\text{He}(\gamma, n)$. They show interesting peak structures based on a complex interplay of all dynamical ingredients.

In relation to the two experimental investigations [1] and [2] we shall show some related point geometry results, but unfortunately are unable to fully analyze those data. This is due to insufficient access to the experimental details. In the present study we shall also compare the theory to existing total $3N$ breakup data on ${}^3\text{He}$ and ${}^3\text{H}$ measured in the low energy region. After finishing this work we heard of ${}^3\text{He}$ breakup data [7], which possibly might be analyzed in the future.

A very recent paper [8] also deals with total photodisintegration cross sections. There, besides studying 3NF effects, the emphasis was placed on performing a benchmark between two totally different approaches: the Faddeev one in momentum space and a hyperspherical harmonic expansion method in configuration space combined with a Lorentz transform method. The results agreed quite nicely documenting the present-day accuracy in treating these quite complicated processes numerically for certain types of nuclear forces and electromagnetic current operators.

We briefly describe our theoretical framework in Sec. II and display our results in Sec. III. The summary is given in Sec. IV.

II. THEORETICAL FRAMEWORK

We refer to Refs. [9–11] for our general notation and specifically to Ref. [5] for the formalism of ${}^3\text{He}$ photodisintegration. As is shown there, the nuclear matrix element

$$N_{\tau}^{3N} \equiv \langle \Psi_{pq}^{(-)} | j_{\tau}(\vec{Q}) | \Psi_{3\text{He}} \rangle \quad (1)$$

for $3N$ breakup of ${}^3\text{He}$ can be written as

$$N_{\tau}^{3N} = \frac{1}{2} \langle \Phi_0 | (tG_0 + 1) P | \tilde{U} \rangle, \quad (2)$$

where $|\tilde{U}\rangle$ obeys the Faddeev-type integral equation

$$|\tilde{U}\rangle = (1+P)j_\tau(\vec{Q})|\Psi_{3\text{He}}\rangle + (tG_0P + \frac{1}{2}(1+P)V_4^{(1)}G_0(tG_0 + 1)P)|\tilde{U}\rangle. \quad (3)$$

We encounter in Eq. (1) the asymptotic relative momenta \vec{p} and \vec{q} of the three final nucleons attached to the $3N$ scattering state $\langle\Psi_{pq}^{(-)}|$ and the spherical component $j_\tau(\vec{Q})$ of the electromagnetic current operator. Further, $\langle\Phi_0|$ is a properly antisymmetrized (in the two-body subsystem) free $3N$ state, t the NN t operator, G_0 the free $3N$ propagator, and P the sum of a cyclical and anticyclical permutation of three particles. Finally, $V_4^{(1)}$ is that part of a $3NF$ which is symmetrical (like the NN t operator) under exchange of particles 2 and 3. That Faddeev equation can be solved rigorously in momentum space using a partial wave decomposition. Any NN force (leading to t) and $3NF$ can be used.

The fivefold differential cross section for the complete ^3He (^3H) breakup is given as

$$\frac{d^5\sigma}{d\Omega_1 d\Omega_2 dS} = \frac{2\pi^2\alpha}{E_\gamma} \frac{1}{2} \sum_{M,m_1,m_2,m_3} (|N_{+1}|^2 + |N_{-1}|^2) \rho_{3N}, \quad (4)$$

where α is the fine-structure constant. In order to avoid kinematical singularities, we represent the breakup cross section along the kinematically allowed locus in the E_1 - E_2 plane and use the arc length S along that locus (on which all events have to lie for fixed Θ_1 , Φ_1 , Θ_2 , and Φ_2) to label the cross section. Then the nonrelativistic phase-space factor is

$$\rho_{3N} = \frac{m_N^2 |\vec{p}_1| |\vec{p}_2|}{\sqrt{\left|1 - \frac{\vec{p}_2 \cdot \vec{p}_3}{|\vec{p}_2|^2}\right|^2 + \left|1 - \frac{\vec{p}_1 \cdot \vec{p}_3}{|\vec{p}_1|^2}\right|^2}}, \quad (5)$$

where the momenta of the two detected nucleons are denoted by \vec{p}_1 and \vec{p}_2 , respectively, and the nucleon mass by m_N .

In view of experiments, which are much easier to perform, we also evaluated the semiexclusive processes $^3\text{He}(\gamma, p)$ and $^3\text{He}(\gamma, n)$. The cross sections are given as

$$\frac{d^3\sigma}{d\Omega_1 dE_1} = \frac{2\pi^2\alpha}{E_\gamma} m_N^2 \frac{1}{2} |\vec{p}_1| |\vec{p}| \mathcal{C} \int d\hat{p} \frac{1}{2} \sum_{M,m_1,m_2,m_3} (|N_{+1}|^2 + |N_{-1}|^2), \quad (6)$$

where $|\vec{p}|$ and \hat{p} are the magnitude (kinematically fixed) and the direction of the relative momentum between nucleons 2 and 3. $\mathcal{C} = \frac{1}{2}$ if the two unobserved particles are identical and $\mathcal{C} = 1$ otherwise.

III. RESULTS

Because of the lack of a full theoretical understanding of nuclear forces, a possible way to search for $3NF$ effects is to

use all present-day high precision NN forces in $3N$ calculations and look for differences between theoretical predictions and data for $3N$ observables. Such searches have already been performed for the binding energies of ^3He , ^3H , and ^4He [12], cross sections and spin observables in elastic nucleon-deuteron scattering [13,14], and in the nucleon induced deuteron breakup process [11,15,16]. The inclusion of various present-day $3NF$ models sometimes removes the differences but sometimes does not. Thus right now the properties of $3NF$'s are still not known. In such a situation all possible information should be used and ^3He photodisintegration is a good additional test ground to search for $3NF$ effects.

We use various dynamical inputs: the high precision NN potential AV18 [17] together with the Urbana IX $3NF$ [18]. That model correctly describes the ^3H binding energy. In our calculations we neglect the pp Coulomb force in the $3N$ continuum but keep it in the ^3He bound state. Except for 21 keV, the binding energy is then the correct one. In addition to the standard nonrelativistic single-nucleon current operator, we employ explicit π - and ρ -like MEC's [19] according to the Riska prescription [20]. They are consistent with dominant parts of AV18 and fulfill the continuity equation in relation to those parts. This has to be improved in the future by adding the remaining pieces to be fully consistent to AV18 in the continuity equation. As an alternative method, we also use the Siegert theorem in the form given in Ref. [6]. Also here improvements are needed in the future to add explicit MEC's to the magnetic multipoles which are not affected by the Siegert approach. Therefore both approaches to many-body currents leave room for improvement. That form does not use long wavelength approximations and is formulated in momentum space. In order to have a first test of the dependence on the choice among the various possible NN and $3NF$ combinations, we also used the NN force CD Bonn [21] plus the modified Tuscon-Melbourne (TM') $3NF$ [22]. That modified force removes deficiencies of the older TM $3NF$ [23], which was in conflict with chiral symmetry [24]. In fact, we use the newest set of parameters for this force, as given in Ref. [25].

In order to search for $3NF$ effects in the $3N$ ^3He photodisintegration, we performed the following investigation. We scanned the whole $3N$ phase space and compared the exclusive breakup cross section based on NN forces only to the one adding $3NF$'s. To that aim, we define the quantity

$$\Delta(\Omega_1, \Omega_2, S) \equiv |d^5\sigma^{\text{NN}+3\text{NF}} - d^5\sigma^{\text{NN}}| / d^5\sigma^{\text{NN}} \times 100\%. \quad (7)$$

In this manner we can associate Δ values to all regions in phase space. Such a search is carried through using two different NN and $3NF$ combinations: AV18 alone and combined with Urbana IX, and CD Bonn alone and together with TM'. Further, in the case of AV18, we work either with the MEC's explicitly or the Siegert approach combined with the single-nucleon current operator. In the case of CD Bonn only the Siegert approach is chosen since consistent MEC's are not available (in any case, they would not be well defined since that NN force has been introduced partial wave per partial

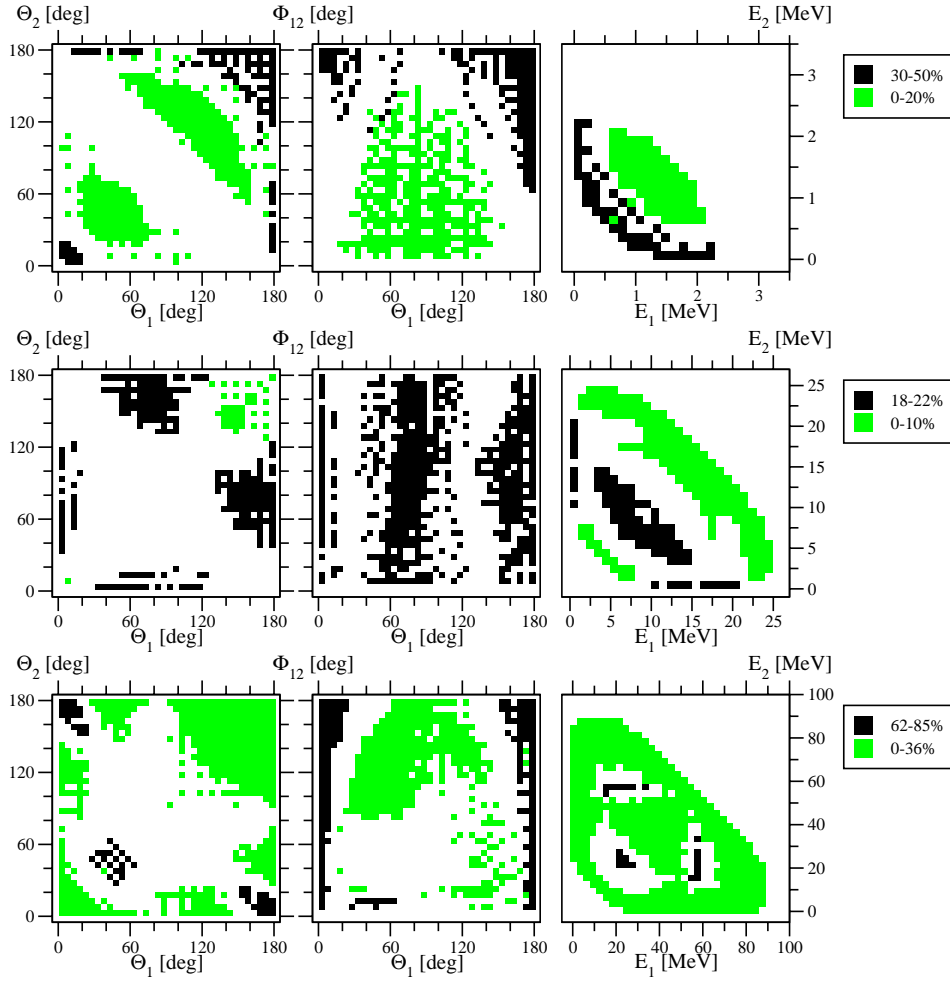


FIG. 1. The regions in the $3N$ phase space projected onto the Θ_1 - Θ_2 , Θ_1 - Φ_{12} , and E_1 - E_2 planes carrying certain values of the quantity Δ from Eq. (7) as indicated in the boxes. That quantity is a measure for $3NF$ effects in $d^5\sigma/d\Omega_1 d\Omega_2 dS$ and varies for the three photon lab energies shown in the first row (12 MeV), the second row (40 MeV), and the third row (120 MeV). The force combination AV18+Urbana IX together with the Siegert approach has been used.

wave). In order to locate phase-space regions uniquely, we show three two-dimensional plots. The first one is the Θ_1 - Θ_2 plane for the two angles of the proton detectors. The second one is the Θ_1 - Φ_{12} plane, where $\Phi_{12} \equiv |\Phi_1 - \Phi_2|$ is the relative azimuthal angle for the two detectors. Finally, the third one is the E_1 - E_2 plane for the correlated energies of the two detected protons. To fill the three planes we proceed as follows. The whole phase space is filled with discrete points corresponding to certain grids in $\Theta_1, \Theta_2, \Phi_1, \Phi_2$, and E_1 . For Θ_1 and Θ_2 fixed we search for the maximal value of Δ in the three-dimensional subspace spanned by Φ_1, Φ_2 , and E_1 . Then we combine those maximal Δ values into three groups and associate certain gray tones to those group values. Next we choose a fixed Θ_1 and $\Phi_{12} = |\Phi_2|$ (one can put $\Phi_1 = 0^\circ$) and search again for the maximal values of Δ in the two-dimensional subspace spanned by Θ_2 and E_1 . The same gray tones and groupings are then applied. Finally, in the E_1 - E_2 plane we search for the maximal Δ values in the three-dimensional subspace spanned by $\Theta_1, \Theta_2, \Phi_{12}$ and repeat the procedure. For a larger number of groups see Ref. [26]. This procedure will be now applied in Figs. 1–4. We performed the investigation for three photon laboratory (LAB) energies $E_\gamma = 12, 40$, and 120 MeV. Please note that in Ref. [26] the NN interaction was taken in the form of np -interaction only, while in the present work we include pp and nn interactions by the “ $\frac{2}{3} + \frac{1}{3}$ ” rule [27].

Figure 1 is based on AV18+Urbana IX and the use of the Siegert’s approach. For the sake of visibility, since we use only gray tones, we split the variations of the quantity Δ into two groups which are explicitly shown and a third one in between which is just white. This is done for each energy. A more refined splitting (shown in color) can be found in Ref. [26]. The first, second, and third rows refer to $E_\gamma = 12, 40$, and 120 MeV, respectively. Based on the meaning of the gray tones, as explained above, one can proceed as follows. Choosing a region in the Θ_1 - Θ_2 plane with a black tone we know that in the Θ_1 - Φ_{12} plane there must exist also black region for the same Θ_1 . This allows to read off a certain value of Φ_{12} . Then the angular positions of the two detectors are fixed, which defines the S curve in the E_1 - E_2 plane. Along such a S curve there must be again a black region, where one can read off the corresponding range of energies. Choosing for instance another combination of tones, like a black one in the Θ_1 - Θ_2 plane, white one in the Θ_1 - Φ_{12} plane one knows that the S curve in the E_1 - E_2 plane lies in the white and maybe gray regions. This should explain the use of Figs. 1–4. Clearly, the biggest $3NF$ effects are for $E_\gamma = 120$ MeV reaching up to 85%. Thus, for instance, for angular configurations $\Theta_1 = \Theta_2 \approx 40^\circ$, $\Phi_{12} \approx 20^\circ$, and for instance, $E_1 \approx 20$ MeV and $E_2 \approx 20$ MeV $3NF$ effects of that big size occur for that nuclear force model and for that choice of the electromagnetic current operator. At E_γ

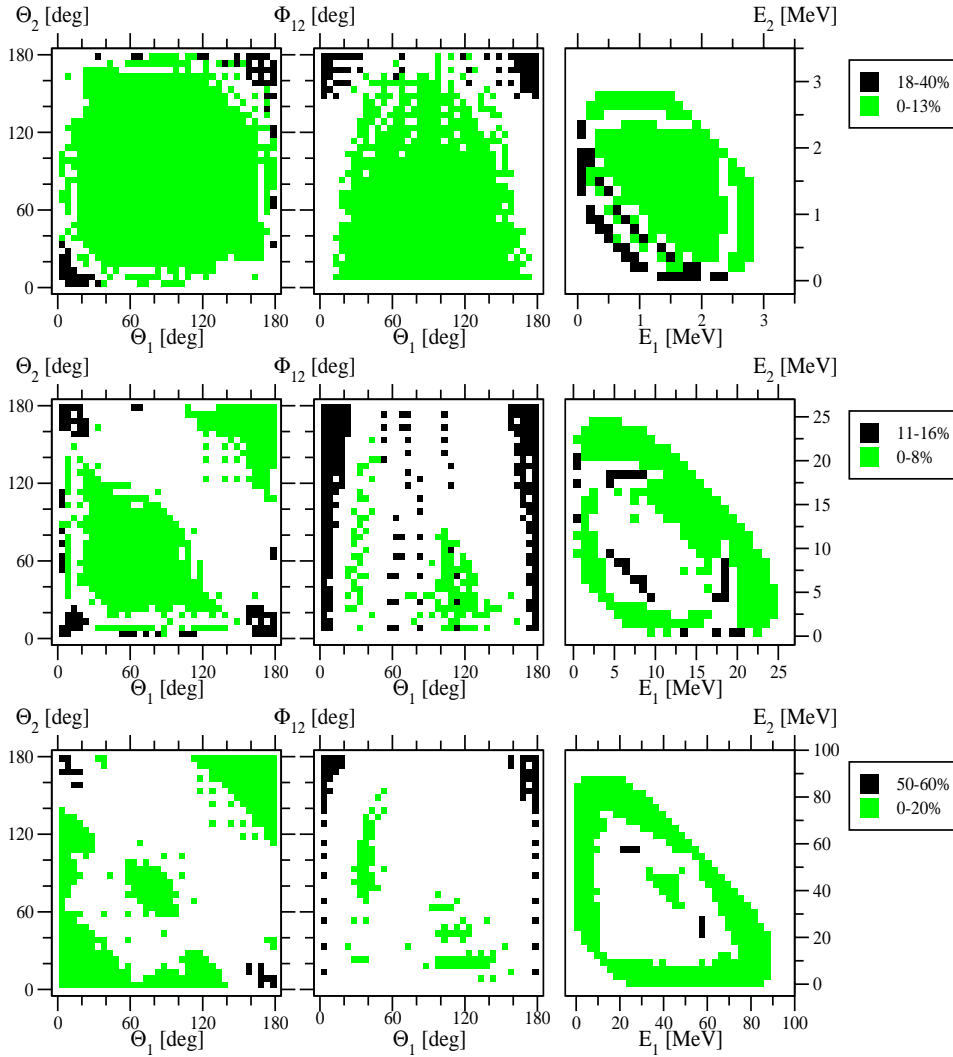


FIG. 2. The same as in Fig. 1, but for the force combination CD Bonn+TM' and the Siegert approach.

$=40$ MeV the effects are significantly smaller, which comes to us as a surprise since they are larger again at 12 MeV. Maybe it is a phenomenon similar to the one as we found in Ref. [5] for the pd breakup process in ^3He photodisintegration. There we saw that 3NF effects essentially vanished around 30 MeV, whereas below and above that energy they were significantly present. Here, at the lowest energy $E_\gamma = 12$ MeV 3NF effects are as large as 50%. The white areas between the dark and gray shaded regions in the two left panels for all three energies refer to Δ values between 20% and 30% in case of $E_\gamma = 12$ MeV and correspondingly for the other energies. In the very right panels the allowed energies E_1 and E_2 are kinematically restricted and events between 20% and 30% for $E_\gamma = 12$ MeV, etc., are present between the dark and gray shaded regions, whereas in the right upper corner there are no events.

This result can now be compared to the choice CD Bonn+TM' in Fig. 2, again using the Siegert approach. For $E_\gamma = 12$ and 120 MeV the outcome is qualitatively similar to Fig. 1, except that for 120 MeV the dark spots around $\Theta_1 = \Theta_2 \approx 40^\circ$, $\Phi_{12} \approx 20^\circ$, and $E_1 = E_2 \approx 20$ MeV are missing. At 40 MeV, where the effects are small, the patterns are nevertheless in reasonable agreement (for a more detailed comparison see Ref. [26]).

Now we ask the question, will the choice of handling MEC's disturb the outcome too strongly? To give a first hint to the answer, we show in Fig. 3 the choice AV18+Urbana IX now together with explicit MEC's instead of Siegert. Comparing to Fig. 1, the patterns are at least qualitatively similar. This is desirable, since both current prescriptions should be close to each other, after all. But there are differences that in a quantitative analysis of future data might be disturbing. This has been quantified by comparing the cross sections underlying Figs. 1 and 3 and locating the phase-space regions where that difference is large or small. We find that at 12 MeV the difference in the two approaches for the currents stays below about 20% in most of the phase-space regions, whereas already at 40 MeV it is roughly only in half of the phase-space region. At 120 MeV the difference is larger. Clearly the question of the choice of the current requires further theoretical investigations which, however, is outside the scope of this paper. We refer the reader to Ref. [26] for more details.

Let us now add two comments. It is important to note that a single-nucleon current operator alone would be totally insufficient. This is a well known fact for photodisintegration. We demonstrate this by defining

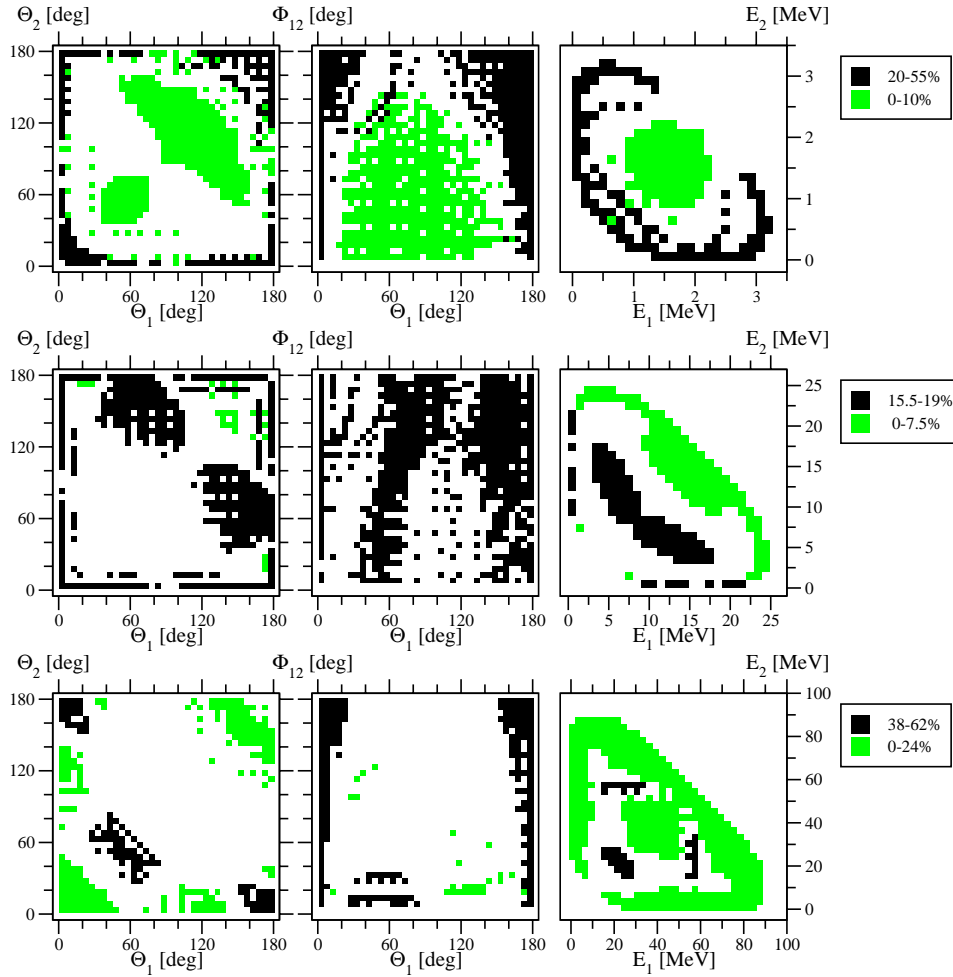


FIG. 3. The same as in Fig. 1, but instead of the Siegert approach explicit MEC's have been used.

$$\Delta'(\Omega_1, \Omega_2, S) \equiv \left| \frac{d^5 \sigma_{MEC}^{NN+3NF}}{d^5 \sigma_{\text{single nucleon}}^{NN+3NF}} - 1 \right| \times 100\% \quad (8)$$

and display the corresponding regions in phase space in Fig. 4. The force combination AV18+Urbana IX has been used. The outcome is clear-cut. In most regions of the phase-space Δ' is much larger than 100% at higher energies. Even at 12 MeV there are many phase-space regions, where using the single-nucleon current operator would be wrong by about 50%.

Often in the literature photodisintegration is treated keeping only the lowest multipole E1. This extreme low energy assumption would be quite insufficient for nearly all phase-space regions and for all three photon energies studied in this paper. This can again be quantified and we find that even at 12 MeV there are plenty of breakup configurations where the electric multipole E1 alone would be wrong by more than 20%. Again, for detailed plots see Ref. [26].

Finally, but quite important for future experiments, we display the regions in phase space where for AV18+Urbana IX based on the Siegert approach and all multipoles (in practice up to E7 and M7) $d^5 \sigma^{NN+3NF}$ takes on certain values. This is shown in Fig. 5. We divided the cross section values

for each photon energy arbitrarily into three groups. Now the white regions contain cross section values below the lowest values explicitly stated. In the Θ_1 - Θ_2 planes the prominent enhancements are along $\Theta_1 \approx \Theta_2$ and $\Theta_2 \approx 180^\circ - \Theta_1$. They are connected to proton-neutron and proton-proton final state interaction peak (FSIP) configurations, respectively. The pp FSIP's occur for small Φ_{12} 's and the pn ones for larger Φ_{12} 's. The FSIP character is clearly documented in the E_1 - E_2 projections with a high energy transfer to one of the nucleons (in case of both E_1 and E_2 low, the high energy transfer is of course to the neutron).

We would like to point to the regions in phase space, where the cross section is large, 3NF effects are large, and the difference in the predictions choosing Siegert or explicit MEC's is small. For a certain quantification of those requirements we display the results in Fig. 6. This should be of special interest for future experiments. In Fig. 6 all three rows are for $E_\gamma = 120$ MeV.

Now we would like to show a few examples for the five-fold differential cross sections directly. First, we regard a case corresponding to Fig. 6, where 3NF effects are large, the difference between the current predictions is small, and the cross section is large. This is shown in Fig. 7. Another extreme and opposite case is displayed in Fig. 8, where the two choices of currents lead to large differences but where 3NF

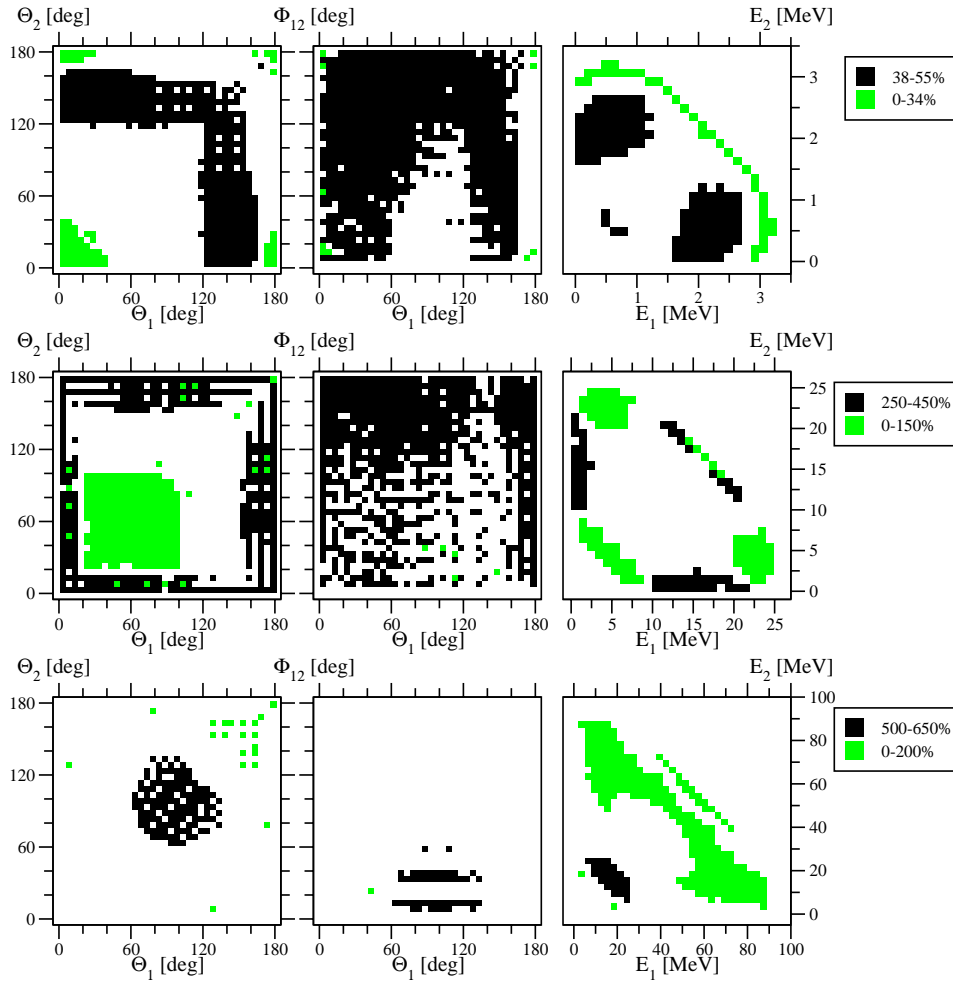


FIG. 4. The same projections of the $3N$ phase space as in Fig. 1, but for the quantity Δ' of Eq. (8). Δ' is a measure of the difference in $d^5\sigma/d\Omega_1 d\Omega_2 dS$ between the use of MEC's and the restriction of the current operator to a single-nucleon one. AV18+Urbana IX has been used.

effects are small. In Fig. 9 we show a case where more than one-body current effects are especially large and finally in Fig. 10 a case where all possible force and current combinations give essentially the same result. Thus we see a great variety in the interplay of forces and currents for different asymptotic configurations. We refer to Ref. [26] for results for $E_\gamma=12$ and 40 MeV and where moreover in addition to ${}^3\text{He}$ also the ${}^3\text{H}$ target has been considered.

Before we compare to a few existing data we would like to show the semiexclusive cross sections for ${}^3\text{He}$ and ejecting either a proton or a neutron. This is displayed in Figs. 11 and 12 for the example $E_\gamma=120$ MeV and for four selected ejection angles. For the other energies, 12 and 40 MeV, see Ref. [26]. We show the following force and current combinations: AV18+single-nucleon current, AV18+Siegert, AV18+MEC, AV18+Urbana IX + Siegert. The 3NF effects are unfortunately rather small. The integration over the two spectator nucleons (the two angles of their relative momenta) for each given nucleon energy $E_{p,n}$ washes out the strong signatures for 3NF's which are located only in part of the integrated phase space, as seen in Fig. 1. Nevertheless, data for this relatively "simple" one-arm experiment would be of interest to test theory in that partially integrated form as we demonstrate now.

For the p ejection we see four peak structures, two of them of the type FSIP. The relative energy of two outgoing

nucleons goes to zero and one sees the enhancement of the NN t -matrix due to the virtual 1S_0 state. The structure, for instance, for $\Theta_p=60^\circ$ at $E_p=20$ MeV is a pp FSIP, which is shifted slightly for the other proton angles. In case of the neutron ejection the corresponding peaks are due to a pn pair. The FSIP's at the highest nucleon energies are due to the not detected pairs, pn for p ejection and pp for n ejection. The pronounced peak around 74 MeV for $\Theta_n=0^\circ$ and the corresponding shifted ones for the other neutron angles are due to a complex interplay of the phase-space factor, enhancement in the ${}^3\text{He}$ wave function due to certain momentum arguments, final state interactions, and two-body currents. To achieve this sort of insight, we looked first into PWIAS¹ alone and using only the single-nucleon current. In that case which allows analytical insight, we found that the enhancement results from small momentum arguments in the ${}^3\text{He}$ wave function (about 1 fm^{-1}). (The momentum dependence of a $3N$ wave function is nicely displayed, for instance, in Ref. [28].) That peak structure in PWIAS survives if one adds the other dynamical ingredients. Thereby we investigated under the full dynamics the individual kinematically complete contributions of the fivefold differential cross

¹PWIAS denotes the fully antisymmetrized plane wave approximation.

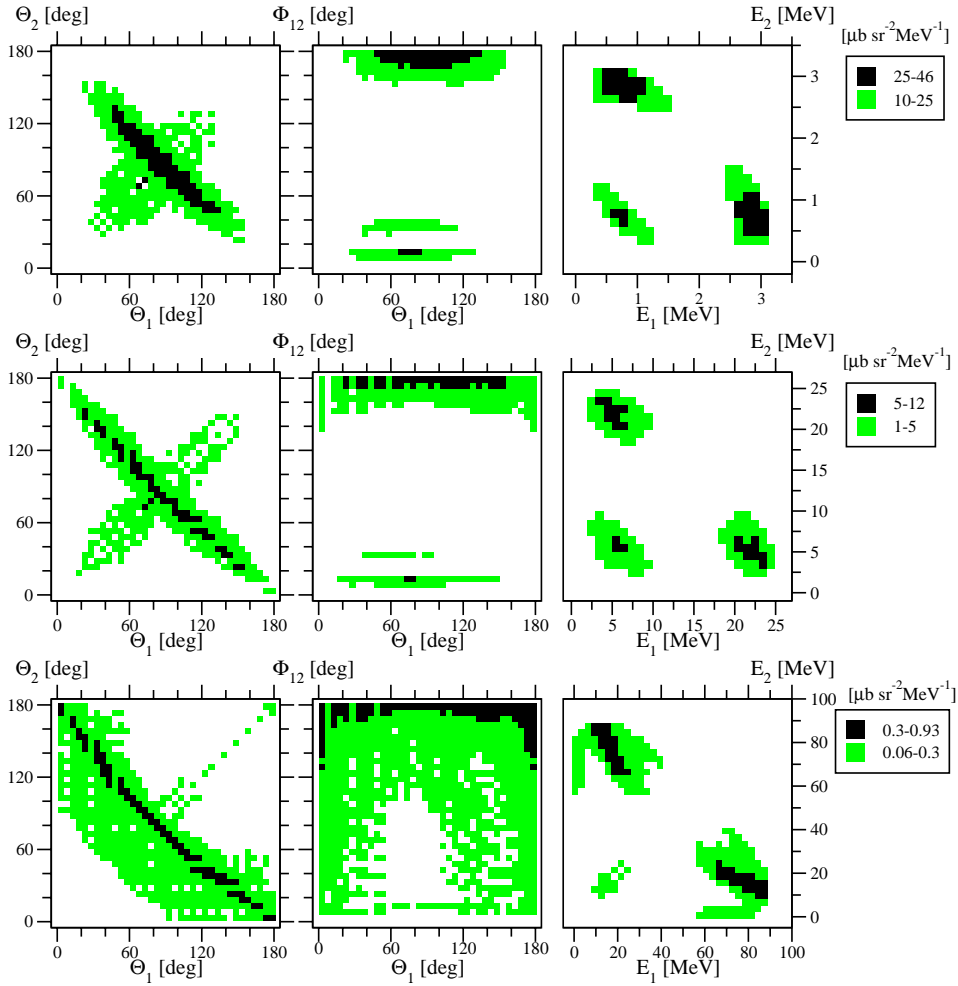


FIG. 5. The same projections as in Fig. 1, but for $d^5\sigma/d\Omega_1 d\Omega_2 dS$ itself. AV18 + Urbana IX together with the Siegert approach has been used.

section to the semiexclusive one in that peak region. We found that the dominant contributions arise from nearly back to back breakup configurations. The neutron is ejected under 0° , to choose one example, and one proton close to 160° with an energy of 34 MeV. The second proton receives very little energy (a few MeV). In case of the proton ejection the corresponding peak around 78 MeV and $\Theta_p=0^\circ$ receives again the dominant contribution from the proton in forward direction and a neutron in backward direction with energies as above. Again the second proton has a very small energy. The peak at the very low proton energy spectrum gets its dominant contribution from a proton-neutron pair emitted roughly back to back and about perpendicular to the photon direction. Each one has about 50 MeV. That peak structure, which is also seen in PWIAS, is absent in case of the n ejection. We could not clarify that point satisfactorily. But we found that if we remove the channels in case of proton ejection where the “spectator pair” of a proton and a neutron interacts in the states 3S_1 - 3D_1 , the peak is dramatically reduced. Such a state is absent for the pp pair in case of the neutron ejection. It is also of interest to point out the fact that those peaks with the underlying structure of back-to-back emission are strongly enhanced by the action of two-body currents. That enhancement is much reduced outside those peak regions. Because of that interesting underlying dynamics, comparison to data would be very welcome.

We do not show the corresponding curves for the semiexclusive process for ${}^3\text{H}$ since they are very similar in shape if proton and neutron are replaced against each other [26].

Now let us finally come to data. As mentioned in the Introduction, there are data [1] for ${}^3\text{He}(\gamma,pp)n$ for photon energies between $E_\gamma=90$ and 250 MeV. Table I of Ref. [1] shows the central proton detection angles for the four angular combinations chosen in that experiment. For fixed angles of the two proton detectors the proton energies are correlated and kinematically allowed events have to lie on a locus, as pointed out before. This corresponds to the representation of the fivefold differential cross section we used before in Figs. 7–10. We show in Figs. 13 and 14 the cross section $d^5\sigma/d\Omega_1 d\Omega_2 dS$ for two examples (LR - RL and LL - RR configurations, using the notation of Ref. [1]) from the four angular combinations studied experimentally in Ref. [1]. Among the four photon energies we looked into ($E_\gamma=80, 100, 120,$ and 160 MeV), only the highest is above the pion threshold. We compare cross sections for AV18 and AV18 + Urbana IX. In all cases the explicit MEC’s have been used. While for the first angular combination 3NF effects are hardly visible, they can be seen for the second angular combination though the effects stay below 25%. The cross sections for the two remaining angular combinations from Ref. [1] (not shown) are somewhere in between and the 3NF ef-

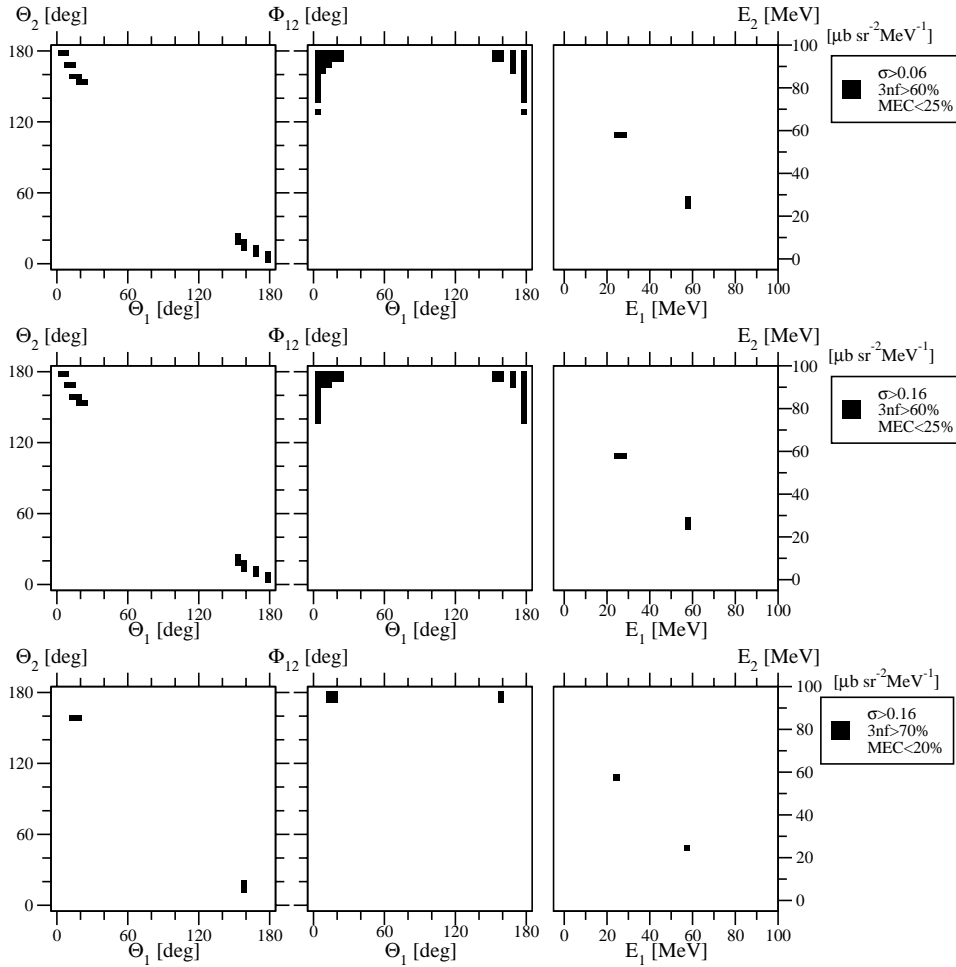


FIG. 6. The same projections as in Fig. 1, but for $d^5\sigma/d\Omega_1 d\Omega_2 dS$ itself for $E_\gamma = 120$ MeV (all three rows). AV18+Urbana IX together with the Siegert approach has been used. The additional conditions ($\sigma > \dots$) onto $d^5\sigma/d\Omega_1 d\Omega_2 dS$ in units of $[\mu\text{b sr}^{-2} \text{MeV}^{-1}]$, onto 3NF effects ($3nf > \dots$) and onto the difference between predictions in the Siegert and explicit MEC approaches ($\text{MEC} < \dots$), are shown in the boxes for each line.

fects are rather small. In principle, these results should be compared to the data. The data of Ref. [1] were, however, integrated over the S curve (see below).

We compare our theory to those integrated cross sections. We took the cuts for the minimal proton energies quoted in

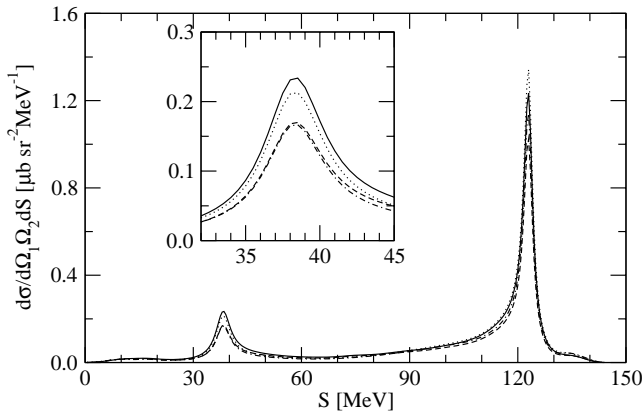


FIG. 7. Fivefold differential cross sections for the angular configuration $\Theta_1 = 142^\circ, \Phi_1 = 0^\circ, \Theta_2 = 27^\circ, \Phi_1 = 180^\circ$, at photon lab energy $E_\gamma = 120$ MeV. The AV18 predictions in Siegert approximation to the nuclear current (explicit MEC) are given by dashed (dash-dotted) curve and corresponding AV18+Urbana IX predictions are given by solid (dotted) curve.

Ref. [1] into account, but no further angular averaging. These data are differential cross sections in both solid angles: $d^4\sigma/d\Omega_1 d\Omega_2$. Figure 15 confronts our theoretical results based on AV18 + MEC and AV18+Urbana IX + MEC to the experimental data from Fig. 9 in Ref. [1]. First of all we see that the 3NF effects are smaller than the error bars and, second, we can only state that we predict the right order of magnitude. The reasonable agreement in case of the first angular combination might be accidental. Certainly, new and precise data would be very welcome and a theoretical analy-

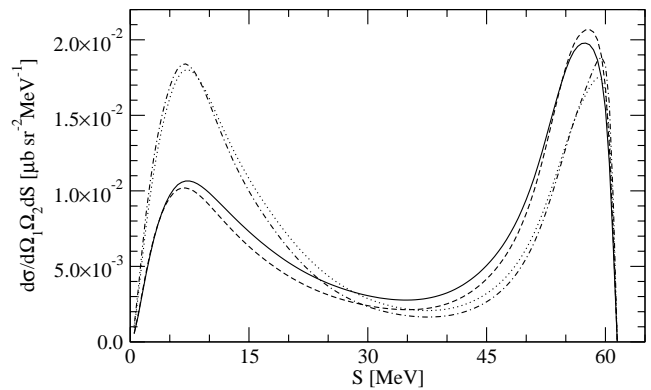


FIG. 8. The same as in Fig. 7, but for $\Theta_1 = 101^\circ, \Phi_1 = 0^\circ, \Theta_2 = 164^\circ, \Phi_1 = 109^\circ$.

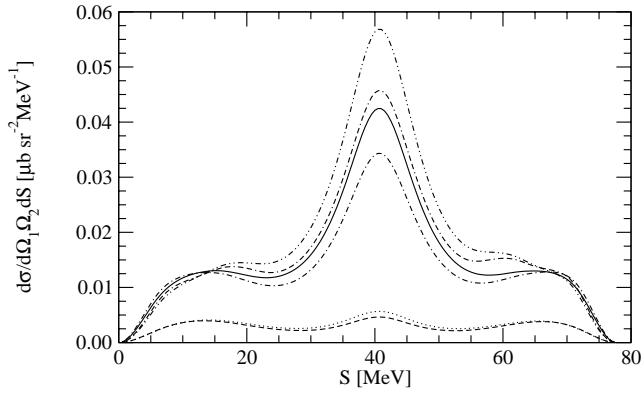


FIG. 9. Fivefold differential cross sections for the angular configuration $\Theta_1=88^\circ$, $\Phi_1=0^\circ$, $\Theta_2=100^\circ$, $\Phi_1=11^\circ$, at photon lab energy $E_\gamma=120$ MeV. The AV18 predictions in single nucleon, Siegert, and explicit MEC approximations to the nuclear current are represented by dashed, dotted-double-dashed, and dash-dotted curves, respectively. The corresponding AV18+Urbana IX predictions are represented by dotted, dashed-double-dotted, and solid curves, respectively.

sis, which takes into account all experimental conditions, should be carried through. We note that we predict much larger 3NF effects for angular combinations according to Fig. 6 (in case of $E_\gamma=120$ MeV).

The second experiment [2] quoted in the Introduction shows ${}^3\text{He}(\gamma,np)$ differential cross sections as a function of the opening angle between the neutron and the proton for $\Theta_p=81^\circ$ in the laboratory frame. We compare our results for two photon energies $E_\gamma=55$ and 80 MeV to this data. No angular averaging whatsoever has been performed in the theory. If we look into Fig. 16 we see again small 3NF effects and find a reasonable agreement with the data except that our peaks are too high. At least partially this might be related to the missing angular averaging and possible further experimental conditions, which we could not take into account.

Finally, in Fig. 17, we compare theory for the total ${}^3\text{He}$ and ${}^3\text{H}$ 3N photodisintegration cross section to data in the low energy region. Some of the results have been shown

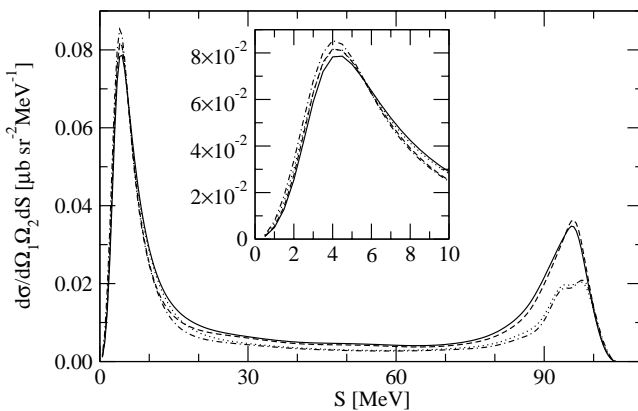


FIG. 10. The same as in Fig. 7, but for $\Theta_1=30^\circ$, $\Phi_1=0^\circ$, $\Theta_2=145^\circ$, $\Phi_1=77^\circ$.

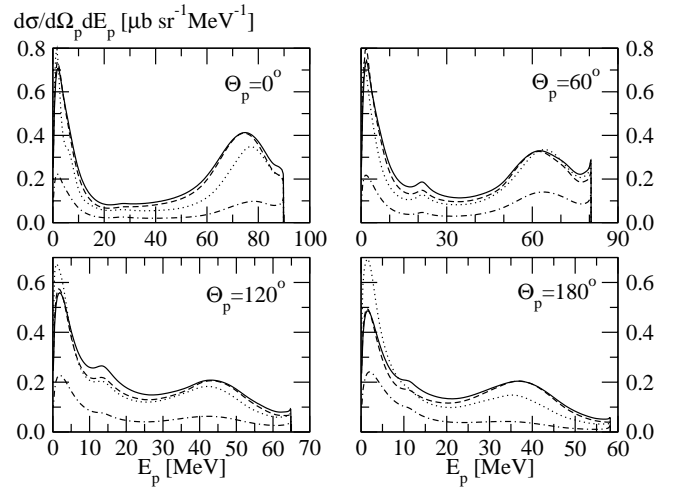


FIG. 11. The semiexclusive cross sections for the process ${}^3\text{He}(\gamma,p)$ for four ejection angles as a function of the proton energy E_p . The solid curve is for AV18+Urbana IX+Siegert, the dashed curve for AV18+Siegert, the dotted curve for AV18+MEC, and the dash-dotted curve for AV18+single-nucleon current operator. The photon energy is $E_\gamma=120$ MeV.

before in Ref. [8]. In both cases theory is roughly inside the bulk of the data and in case of ${}^3\text{H}$ the 3NF effects seem to be favored by the data. Unfortunately, the quality of the data is not too high and precise data at low and higher energies are badly missing.

IV. SUMMARY

We performed Faddeev calculations for the ${}^3\text{He}$ photodisintegration into three nucleons. The NN forces AV18 and CD Bonn in combination with the 3NF's Urbana IX and TM' have been applied. Results are presented for photon energies $E_\gamma=12$, 40 , and 120 MeV as representative examples. We scanned the whole phase space for 3N breakup to search for regions where 3NF effects show up significantly. We found

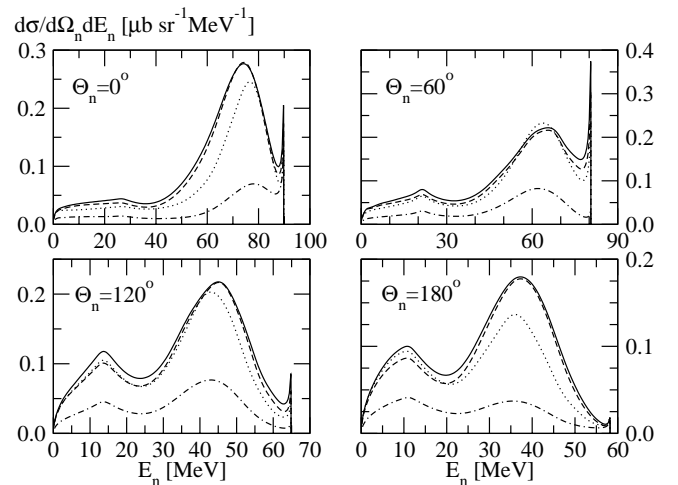


FIG. 12. The semiexclusive cross sections for the process ${}^3\text{He}(\gamma,n)$ for four ejection angles as a function of the neutron energy E_n . Curves as in Fig. 11.

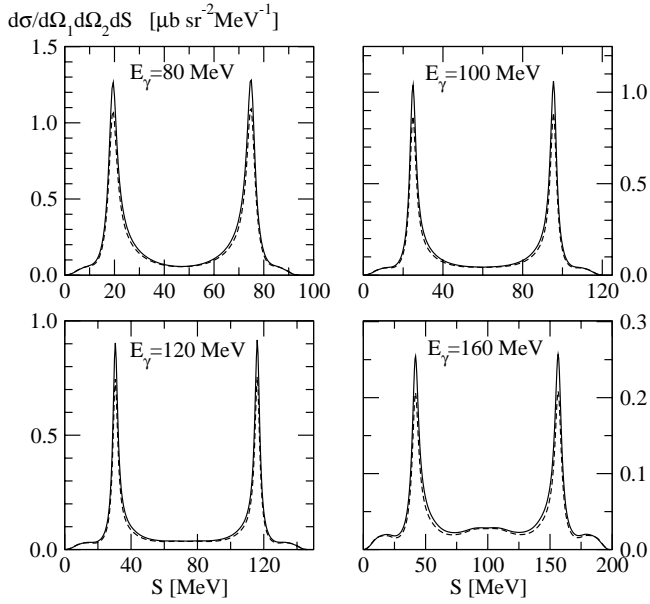


FIG. 13. Fivefold differential cross sections for the angular configuration $LR-RL$ of Ref. [1] ($\Theta_1=81.0^\circ, \Phi_1=0.0^\circ, \Theta_2=80.3^\circ, \Phi_2=180.0^\circ$) along the S curve for the photon energies $E_\gamma=80, 100, 120,$ and 160 MeV. The predictions for AV18 (dashed curve) and AV18+Urbana IX (solid curve) are compared.

effects as large as 85% which should be checked experimentally. We also found that two-body currents are extremely important and the restriction to a single-nucleon current would be rather meaningless. We use explicit π - and ρ -like exchange currents consistent to the NN force AV18 as well as the Siegert approach without long wavelength approximation. Both currents lead qualitatively to the same results but not quantitatively, which clearly calls for an improved future treatment. Precise future data for that complete ${}^3\text{He}$ breakup

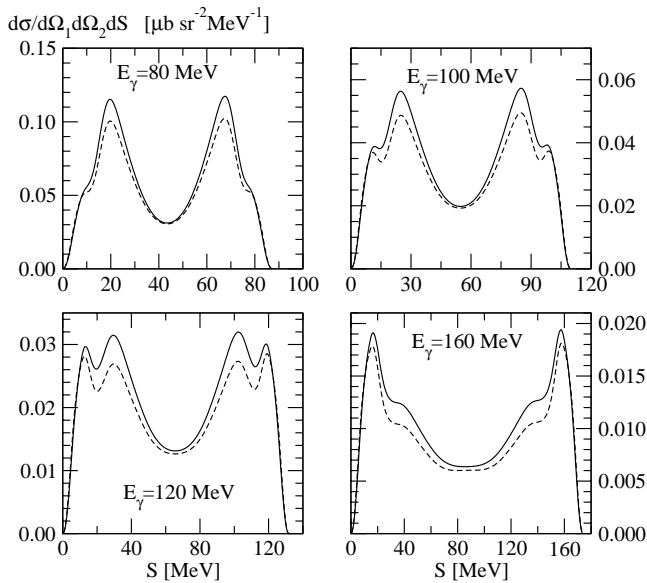


FIG. 14. The same as in Fig. 13, but for the angular configuration $LL-RR$ of Ref. [1] ($\Theta_1=92.2^\circ, \Phi_1=0.0^\circ, \Theta_2=91.4^\circ, \Phi_2=180.0^\circ$).

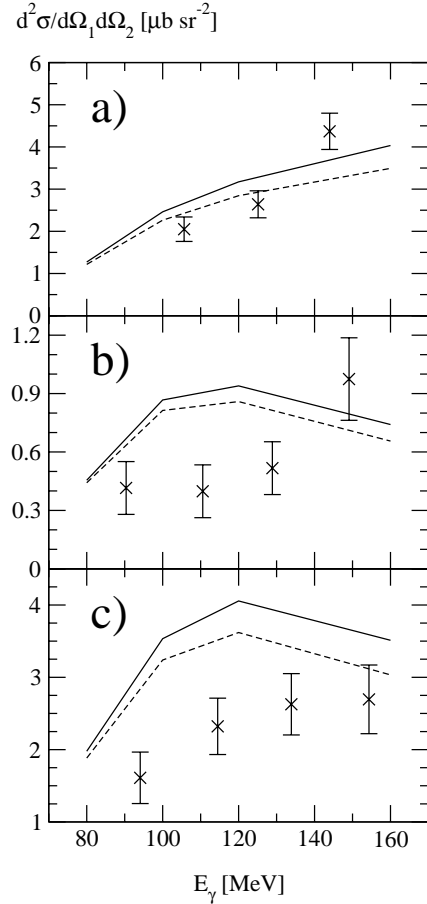


FIG. 15. The fourfold differential cross sections $d^4\sigma/d\Omega_1 d\Omega_2$ for the ${}^3\text{He}(\gamma,pp)n$ process as a function of E_γ in comparison to data given in Fig. 9 of Ref. [1] for the angular configurations $LR-RL$ (a), $LL-RR$ (b), and $LL-RL+LR-RR$ ($\Theta_1=91.7^\circ, \Phi_1=0.0^\circ, \Theta_2=80.9^\circ, \Phi_2=180.0^\circ$) and ($\Theta_1=81.5^\circ, \Phi_1=0.0^\circ, \Theta_2=90.8^\circ, \Phi_2=180.0^\circ$) (c). The solid curve is for AV18+Urbana IX +MEC, the dashed curve for AV18+MEC.

preferably for all of the phase space would be very useful to check the present day nuclear dynamics and the choice of the electromagnetic current operator. Those data would supplement the search for 3NF effects going on in $3N$ scattering [13–16].

In addition, we predicted cross sections for the semiexclusive processes ${}^3\text{He}(\gamma,p)$ and ${}^3\text{He}(\gamma,n)$, where interesting peak structures occur in the energy dependence of the knocked out nucleon.

Finally, we compared theory to data for the exclusive ${}^3\text{He}$ breakup process. The comparison was unfortunately hindered by the fact that, due to the lack of information, we were not able to take the experimental conditions (acceptances in energy and angular resolutions, etc.) into account. Nevertheless, the at least qualitative agreement with the data shows that a proper analysis of new data would be very valuable to find out how well theory describes the complex interplay of NN and $3NF$'s with the absorption mechanism of the photon.

The comparison with the total ${}^3\text{He}$ breakup data was also inconclusive because the available data below 30 MeV have

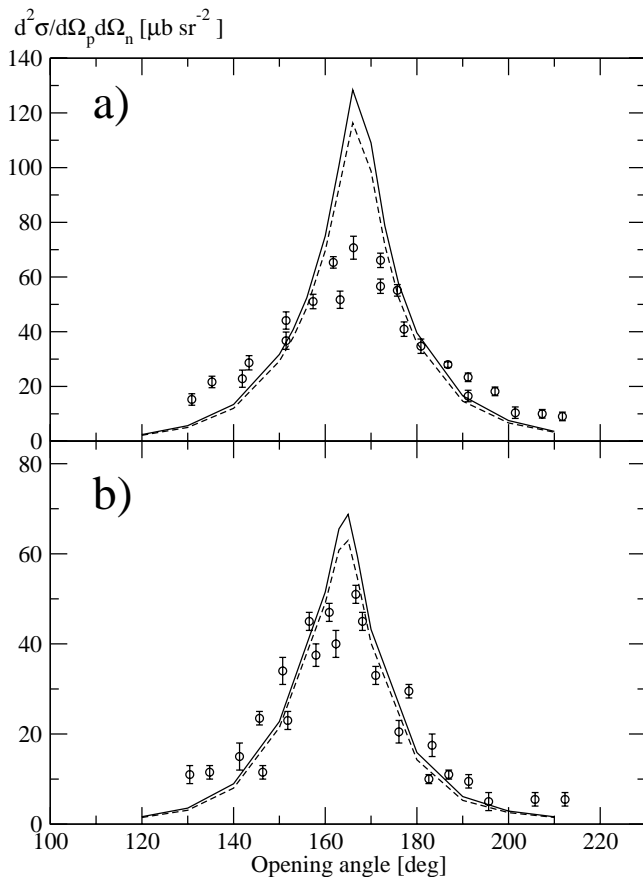


FIG. 16. The fourfold differential cross sections $d^4\sigma/d\Omega_1 d\Omega_2$ against the opening angle at $E_\gamma=55$ (a) and 80 MeV (b) for the ${}^3\text{He}(\gamma,pn)p$ process in comparison to data from Ref. [2]. The data in (b) are taken for $E_\gamma=85$ MeV. Solid and dashed curves as in Fig. 15.

large error bars and do not agree with each other. Also, data above 30 MeV are needed.

ACKNOWLEDGMENTS

This work was supported by the Deutsche Forschungsgemeinschaft (J.G., R.S.), the Polish Committee for Scientific

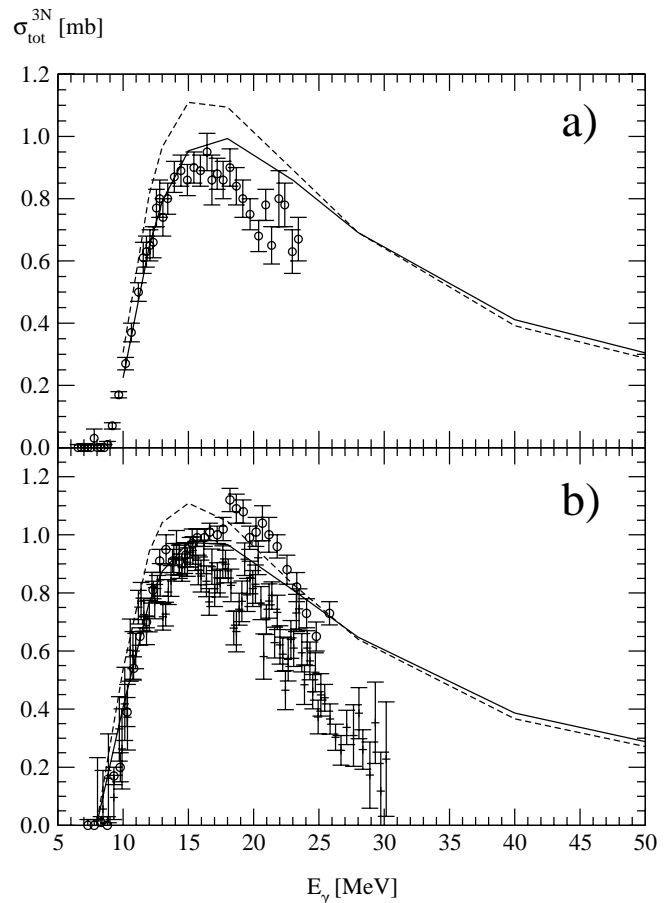


FIG. 17. The total breakup cross sections for ${}^3\text{H}$ (a) and ${}^3\text{He}$ (b) photodisintegration in comparison to data. The solid curve refers to AV18+Urbana IX, the dashed curve to AV18 alone, both in combination with the Siegert approach. Data in (a) are taken from Ref. [29] and in (b) from Refs. [29] (circles) and [30] (pluses).

Research under Grant Nos. 2P03B02818 and 2P03B05622, and by NFS Grant No. PHY0070858. R.S. acknowledges financial support of the Foundation for Polish Science. The numerical calculations have been performed on the Cray T90, SV1, and T3E of the NIC in Jülich, Germany.

[1] A.J. Sarty *et al.*, Phys. Rev. C **47**, 459 (1993).
 [2] N.R. Kolb *et al.*, Phys. Rev. C **44**, 37 (1991).
 [3] J.M. Laget, Nucl. Phys. **A497**, 391 (1989), and references therein.
 [4] B.F. Gibson and D.R. Lehman, Phys. Rev. C **13**, 477 (1976).
 [5] R. Skibiński, J. Golał, H. Kamada, H. Witała, W. Glöckle, and A. Nogga, nucl-th/0204024.
 [6] J. Golał *et al.*, Phys. Rev. C **62**, 054005 (2000).
 [7] P.T. Debevec (private communication).
 [8] J. Golał, R. Skibiński, W. Glöckle, H. Kamada, A. Nogga, H. Witała, V.D. Efros, W. Leidemann, G. Orlandini, and E.L. Tomasiak, Nucl. Phys. **A707**, 365 (2002).

[9] W. Glöckle, *The Quantum Mechanical Few-Body Problem* (Springer-Verlag, Berlin, 1983).
 [10] J. Golał, H. Kamada, H. Witała, W. Glöckle, and S. Ishikawa, Phys. Rev. C **51**, 1638 (1995).
 [11] W. Glöckle, H. Witała, D. Hüber, H. Kamada, and J. Golał, Phys. Rep. **274**, 107 (1996).
 [12] A. Nogga, H. Kamada, and W. Glöckle, Phys. Rev. Lett. **85**, 944 (2000).
 [13] H. Witała *et al.*, Phys. Rev. C **63**, 024007 (2001), and references therein.
 [14] K. Sekiguchi *et al.*, Phys. Rev. C **65**, 034003 (2002).
 [15] J. Kuroś-Żolnierczuk, H. Witała, J. Golał, H. Kamada, A.

- Nogga, R. Skibiński, and W. Glöckle, Phys. Rev. C **66**, 024003 (2002).
- [16] J. Kuroś-Żolnierczuk, H. Witała, J. Golak, H. Kamada, A. Nogga, R. Skibiński, and W. Glöckle, Phys. Rev. C **66**, 024004 (2002).
- [17] R.B. Wiringa, V.G.J. Stoks, and R. Schiavilla, Phys. Rev. C **51**, 38 (1995).
- [18] B.S. Pudliner, V.R. Pandharipande, J. Carlson, Steven C. Pieper, and R.B. Wiringa, Phys. Rev. C **56**, 1720 (1997).
- [19] V.V. Kotlyar, H. Kamada, J. Golak, and W. Glöckle, Few-Body Syst. **28**, 35 (2000).
- [20] D.O. Riska, Phys. Scr. **31**, 107 (1985); **31**, 471 (1985).
- [21] R. Machleidt, F. Sammarruca, and Y. Song, Phys. Rev. C **53**, R1483 (1996).
- [22] J.L. Friar, D. Hüber, and U. van Kolck, Phys. Rev. C **59**, 53 (1999).
- [23] S.A. Coon *et al.*, Nucl. Phys. **A318**, 242 (1979); S.A. Coon and W. Glöckle, Phys. Rev. C **23**, 1790 (1981).
- [24] H. Kamada, D. Hüber, and A. Nogga, Few-Body Syst. **30**, 121 (2001).
- [25] A. Nogga, H. Kamada, W. Glöckle, and B. Barrett, Phys. Rev. C **65**, 054003 (2002).
- [26] R. Skibiński, Ph.D. thesis, Jagiellonian University, Kraków, 2002, <http://www.if.uj.edu.pl/ZFJ/prj/thfewbod.htm>
- [27] H. Witała, W. Glöckle, and H. Kamada, Phys. Rev. C **43**, 1619 (1991).
- [28] Ch. Elster, W. Schadow, A. Nogga, and W. Glöckle, Few-Body Syst. **27**, 83 (1999).
- [29] D.D. Faul, B. Berman, P. Meyer, and D. Olson, Phys. Rev. C **24**, 849 (1981).
- [30] B. Berman, S. Fultz, and P. Yergin, Phys. Rev. C **10**, 2221 (1974).